Available online at www.sciencedirect.com
SCIENCE DIRECT®
International Journal of Thermal Sciences 45 (2006) 284–298
International Journal of Thermal Sciences
www.elsevier.com/locate/ijts

Identification of unifying heat transfer mechanisms along the entire boiling curve

Torsten Lüttich [a], Wolfgang Marquardt [a,*], Martin Buchholz [b], Hein Auracher [b]

[a] *Lehrstuhl für Prozesstechnik, RWTH Aachen, D-52064 Aachen, Germany*
[b] *Institut für Energietechnik, TU-Berlin, D-10587 Berlin, Germany*

Received 22 December 2003; received in revised form 27 April 2004; accepted 27 April 2004

Available online 10 October 2005

Abstract

The interfacial geometry and the associated heat transfer mechanisms close to and at the boiling surface are identified rigorously along the entire boiling curve from wall temperature and two-phase flow sensor probe data taken during boiling of isopropanol. It is conjectured, that the liquid–vapor interface of the wetting structure provides the key mechanism for heat removal due to evaporation along the entire boiling curve. Local fluctuations of surface temperature superheat and heat flux are inferred by the solution of a two-dimensional inverse heat conduction problem employing wall temperature data. Peak heat fluxes of several $MW \cdot m^{-2}$ are estimated. In a next step, the interfacial geometry close to the surface is identified. It is shown that the size of the dry spots and the nucleation site density are well connected to the vapor fraction and the interfacial area density as well as to the contact angle of the wetting fluid. Further, we show that a suitably designed single four-sensor optical probe could provide the necessary data required to *exactly* identify the wetting structure using the wetting structure geometry model proposed here. We further find that interfacial area density accounts for the contact angle of the fluid and correlates well with the boiling heat flux. In conclusion, the results show that essential mechanisms of heat removal along the entire boiling curve can be attributed to interfacial presence and evolution. A single measure, namely the interfacial area density, is suspected to provide the essential mechanism of the heat removal in the boiling process. Finally, the results are discussed with respect to the candidate models for the interfacial geometry and heat transfer mechanisms proposed in the literature. Only, specifically designed and refined boiling experiments as well as identification methods along the line presented in this paper are needed to further verify this postulate.

Keywords: Boiling; Microlayer theory; Multi-phase flow averaging theory; Inverse heat conduction problem; Identification; Interfacial area density; Contact angle; Wetting

1. Introduction

For a reliable design of boiling heat transfer equipment, predictive heat flux correlations are essential. These correlations must adequately capture the governing physical phenomena. Despite many decades of boiling research the mechanistic understanding of boiling processes is still not sufficient to develop models of high prediction quality. Especially in the high heat flux nucleate and transition boiling regions, major physical effects have not yet been captured adequately. As a result, most design methods are currently based on correlations which are valid only in a limited range for one of the boiling regimes. Boiling heat flux has been correlated with different quantities, e.g. superheat, nucleation site density or bubble diameter in nucleate boiling and average vapor fraction or vapor velocity in transition boiling [1]. There are many other correlating parameters. It has been unclear yet which of the parameters is most important in determining boiling heat transfer.

Well established theoretical approaches to develop more detailed mechanistic models of boiling heat transfer claim one or an other mechanism of evaporation at the liquid–vapor interface to play an important role. Two candidates are the microlayer theory proposed by Stephan and Hammer [2] or the unifying framework for nucleate and transition boiling presented by Dhir and Liaw [3]. The basic idea behind the microlayer theory in

* Corresponding author.
E-mail address: marquardt@lpt.rwth-aachen.de (W. Marquardt).

1290-0729/$ – see front matter
doi:10.1016/j.ijthermalsci.2004.04.017

Nomenclature

A_H	total area of heater surface
A_i	interfacial area density
C	parameter
$\bar{C}$	parameter
d_S	equivalent dry patch size
f	arbitrary smooth function or frequency
g	geometry function
$\mathbf{G}$	transfer function matrix
j	index
k	index
L	equivalent dry patch distance
L_i	interfacial line density
$\mathbf{n}$	normal vector
n	number
N	equivalent number of dry patches
$\mathbf{N}$	noise in Laplace domain
$\mathbf{N}_s$	matrix of unit vector of measuring direction
N_p	number of phase changes
$\mathbf{p}$	vector of equivalent key geometrical quantities
q	heat flux
$\hat{q}$	estimated heat flux
$\mathbf{Q}$	heat flux in Laplace domain
$\widehat{\mathbf{Q}}$	estimated heat flux in Laplace domain
$\mathbf{s}$	vector pointing from one sensor to another sensor
s	Laplace domain variable
t	time
$\mathbf{t}$	tangential vector
T	temperature in Laplace domain
v_C	characteristic velocity of interface
$\mathbf{v}$	velocity vector
$\mathbf{x}$	coordinate vector
X	phase indicator function
$\mathbf{y}$	vector of averaged key interfacial quantities
z	coordinate perpendicular to heater surface

Subscripts

0	at heater surface, i.e. $z = 0$
B	boiling surface
fluc	fluctuations
F	filter
i	interface
j	index
k	index
l	index
L	liquid phase
m	index
M	measured
N	nodes
Q	heat flux
s	sensor
V	vapor phase

Greek symbols

α	volume or time fraction or filter parameter
Δs	distance between sensor tips
$\Delta\tau$	appropriate time interval
ΔT	superheat
Δz	distance to heater surface
ν	normal velocity
ν_s	vector of sensed normal velocities
ϕ	contact angle
Φ	basis function

boiling is closely related to works of Wayner [4] who studies spreading liquid films on solid surfaces under non-boiling heat transfer conditions.

The microlayer theory predicts that most of the heat during boiling is transferred in the micro-region of the three-phase contact line by evaporation [2]. As depicted in Fig. 1, the microregion consists of a wedge-shaped liquid meniscus. The microregion itself is a thin liquid film with a typical thickness in the order of 10^{-1} μm. It extends from an adsorbed molecular film at the heater wall below the bubble to a liquid region separating the vapor phase of the bubble from the heated wall. In the microregion, the evaporation mechanism is governed by the capillary forces of adhesion (or "disjoining pressure forces") and surface tension as well as the molecular kinetic heat resistance. The microlayer theory postulates that the molecular heat resistance at the interface dominates the overall heat resistance in the wedge-shaped liquid meniscus.

Dhir and Liaw [3] propose a macroscopic geometry model of "vapor stems" in order to develop a unifying framework for nucleate and transition boiling. Their model assumes that all the heat conducted into the liquid adjacent to the surface is used for evaporation at the interface of the vapor stems. The stems

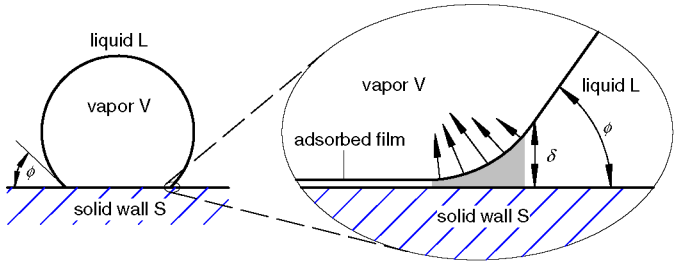

Fig. 1. Micro-region at the three-phase contact line.

have been assumed stationary. In comparison to the microlayer theory, curvature of the interfacial geometry has been neglected in the stem model, but the contact angle is accounted for.

The relevance of the interfacial geometry (bubbles, vapor stems etc.) and the associated transfer phenomena close to the boiling surface has been pointed out in these approaches. However, neither of the two models has been fully validated yet. In particular, in order to predict heat transfer coefficients based on the mechanisms proposed in the microlayer theory, nucleation site densities and bubble departure diameters are needed. At low heat fluxes, nucleation site densities can be obtained from ex-

periments by visual observation of the boiling process. Bubble departure diameters can be calculated by means of growth and force balance models such that the line density at the boiling surface can be determined and the heat transfer coefficients can be well predicted. However, these predictions become less accurate at higher heat fluxes as it is difficult to include the mutual interaction of the bubbles in the model. The geometry model of Dhir and Liaw [3] is used to extrapolate the nucleate boiling curve into transition boiling by employing vapor fraction measurements, but much uncertainty is present in their results. Only a limited data basis is employed in their study and the data, such as the nucleation site density, is taken from simple correlations obtained in different studies. Furthermore, their assumption on the existence of stationary vapor stems can be ruled out from experimental evidence provided by Hohl et al. [5,6] and Buchholz et al. [7]. Therefore, it remains still questionable if these candidate geometries and mechanisms could happen to play a crucial role along the entire boiling curve. Hence, there is still no agreement on a *verified geometry of the wetting structure and the heat transfer mechanisms* valid along the entire boiling curve.

The authors have suggested recently [8] to systematically combine modeling and experimental analysis on a matching scale of resolution with identification techniques to investigate the geometry of the wetting structure close to the boiling surface and the resulting heat transfer mechanism. A methodology to derive such a unifying model has been presented. Interfacial geometry models for the wetting structure and optical probe measurement techniques have been interpreted in terms of multiphase flow averaging theory [9–11]. The wetting structure of FC-72 has been rigorously identified from data obtained with a single sensor optical probe [5]. A sufficiently simple geometry model complying with the limited *experimental resolution* has been employed for this purpose. The contact frequency measured by the probe has been interpreted as a measure for the interfacial area density or its flux subject to a single quantity which is related to an interfacial velocity and which cannot yet be observed experimentally. A strong correlation of the contact frequency with boiling heat flux has also been shown. It was therefore concluded that the volumetric density of vapor–liquid interface and the induced fluctuations due to its movement very close and at the boiling surface play a decisive role in the overall boiling process.

In this paper, the same line of reasoning is pursued using new experimental data taken during pool boiling of isopropanol in order to prove or disprove the modeling hypothesis. The investigations in this paper are further extended to the heated wall. The relevant experimental data for this study is obtained by the pool boiling experiments at 1.0 MPa in an experimental setup which is only briefly described here. Details can be found in [7]. The test heater of the setup is made of copper with 35 mm diameter and 7 mm thickness. At the center of a test heater an array of 36 microthermocouples is implanted within an area of 1 mm^2 by sputtering a 2.5 μm-thin layer of copper and a 1.0 μm-thin layer of gold. It provides temperature fluctuations of the boiling process at a sampling rate of 7.5 kHz. A micro optical probe made from a single mode quartz glass fiber with a tip diameter

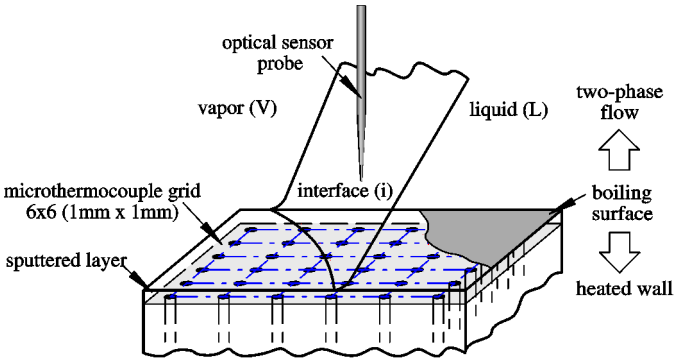

Fig. 2. Identification and experimentation close to the boiling surface.

of less than 1.5 μm delivers information on liquid–vapor fluctuations due to the boiling process as close as 8 μm to the boiling surface at a sampling rate of 200 kHz. Hence, measurements with high temporal and spatial resolution are conducted close to but not at the boiling surface in the two-phase layer and in the heated wall. The overall system, consisting of the two-phase vapor–liquid layer, the boiling surface and the heated wall together with the measurement instrumentation relevant for the model-based identification of basic boiling mechanisms close to the surface is shown in Fig. 2.

The measurements of the wall temperatures and vapor–liquid fluctuations are corresponding on the macroscale since they have been obtained in the same experimental setup at the same operating conditions. Since it has not yet been possible to exactly match the location of the thermocouple array with the probe position except for the axial direction of the probe during the experiments, the measurements are not corresponding on the microscale, i.e. on the scale of single events. Therefore, we have to decouple modeling and identification in the heated wall and in the two-phase flow.

The paper is organized as follows. In the first part, spatial distributions of the heat flux at the boiling surface are identified from local temperature measurements below the surface by the solution of a two-dimensional inverse heat conduction problem. In the second part, the methodology for the identification of the vapor–liquid interfacial geometry introduced in [8] is refined to use four-sensor probe data which is not yet available. Four-sensor probing techniques are shown to yield all information to rigorously identify the wetting structure including the contact angle close to and at the boiling surface. The interfacial geometry is then identified at a distance of 8 μm above the surface using a simple interface geometry model for the entire boiling curve as in [8] employing single sensor probe data. Finally, the contact frequency is again used to correlate the entire isopropanol boiling curve. The results are finally discussed in the context of the mechanisms proposed in the models of Stephan and Hammer [2] and of Dhir and Liaw [3].

2. Estimation of surface heat fluxes

Distinct local temperature fluctuations immediately below the surface have been measured by an implanted array of microthermocouples (see Fig. 2) as presented in the companion

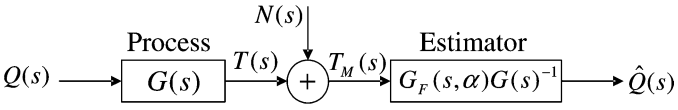

Fig. 3. Filter-based regularization in the frequency domain.

paper [7]. The fluctuations inside the heater are an obvious consequence of the highly localized mechanisms of the boiling process at the boiling surface. They reflect the local surface heat fluxes which we would like to identify for a better understanding of boiling. Even though a very thin layer of sputtered gold and copper is used to cover the microthermocouple tips and to form the boiling surface, the measured temperature fluctuations are thermally damped and influenced by lateral heat conduction. One can therefore expect that they differ from the real temperature variations at the boiling surface. Therefore, the heat fluxes and temperatures at the surface have to be estimated as a function of temporal and spatial coordinates from the measured temperatures below the boiling surface by solving an inverse heat conduction problem (IHCP). This inverse problem is mathematically ill-posed in the sense of Hadamard [12]. In particular, small perturbations in the measured data may lead to large deviations in the estimated quantities. In order to get useful estimates, regularization of the ill-posed problem is necessary [13]. In this work, the solution of an IHCP is accomplished by using the exact inverse transfer function matrix $\mathbf{G}^{-1}(s)$ of a spatially discretized heat conduction model followed by a regularizing low-pass filter to generate a stable approximate inverse. The general solution approach is graphically depicted in Fig. 3.

The low-pass-filter $\mathbf{G}_F(s,\alpha)$ is designed such that the heat flux estimate

$$\widehat{\mathbf{Q}}(s) = \mathbf{G}_F(s,\alpha)\mathbf{G}^{-1}(s)\mathbf{T}_M(s) \tag{1}$$

obtained from temperature measurements $\mathbf{T}_M(s)$ corrupted by noise $\mathbf{N}(s)$ approximates the true heat flux $\mathbf{Q}(s)$ as good as possible. The solution method is described in detail in [14]. It is an extension of a method originally suggested by Tikhonov and Arsenin [15] and tailored to heat conduction problems by Blum and Marquardt [16,17]. It deals with complex geometries, considers optimal boundary parameterization, sensor placement and model reduction in a unified framework, and it addresses their effect on the quality of the estimates [14].

Before the estimation according to Eq. (1) can be carried out, a transfer function matrix $\mathbf{G}(s)$ of the heat conductor relating the measured temperatures $\mathbf{T}_M(s)$ to the surface heat fluxes $\mathbf{Q}(s)$ in the frequency domain,

$$\mathbf{T}_M(s) = \mathbf{G}(s)\mathbf{Q}(s) \tag{2}$$

must be obtained. This involves several steps, i.e. (i) the formulation of a state space model generated from a two-dimensional spatial finite element discretization of the heater encompassing the microthermocouple array, (ii) parameterization of the unknown boundary heat fluxes $\widehat{\mathbf{Q}}(s)$ using linear functions and (iii) order reduction of the discretized model. As shown in [14], modeling and filter design must be suitably adjusted to each other in order to obtain the best possible estimates.

The derivation of the transfer function model (2) for the part of the heater wall implanting the microthermocouple array is discussed in more detail in the following. The goal here is to resolve the high frequency components of the heat flux fluctuations contained in the measured signal during the solution of the IHCP to the extent possible while keeping the discretized model size computationally tractable.

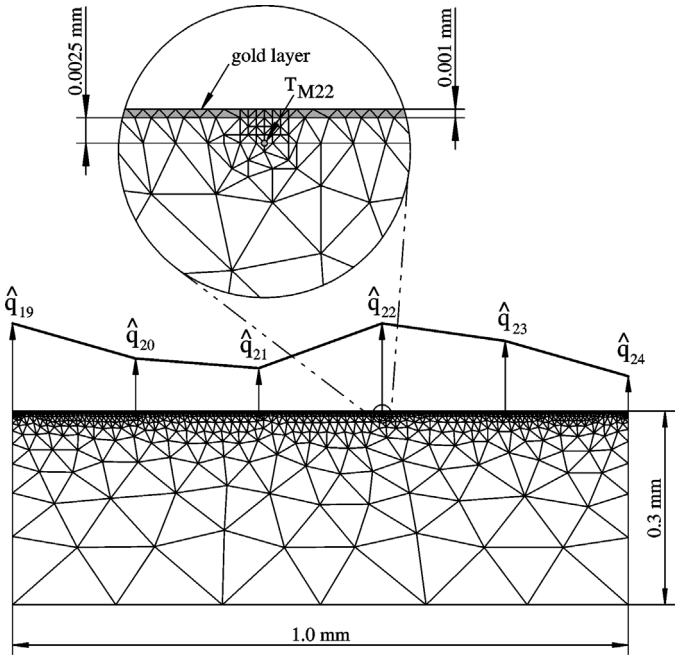

Fig. 4. Two-dimensional finite element model of a row of six microthermocouples with linear parameterization of the unknown surface heat fluxes.

2.1. Finite element model of the heater

For the estimation of the unknown surface heat fluxes and temperatures, a two-dimensional finite element model of the heater with an embedded row of six microthermocouples on a 6×6 array is set up. The boundary conditions of the heater model account for boiling heat transfer at the heater surface and assume zero heat flux at the remaining three boundaries due to a lack of better information. The discretized model is shown in Fig. 4. The two-dimensional domain is perpendicular to the heater surface and contains the row with microthermocouples 19 to 24 [7]. The discretization of the heater model is performed with triangular elements on a non-uniform grid which is locally refined around the microthermocouple locations. The refinement allows to represent the sensor position in the model with an accuracy which complies with the dimensions of the thin gold and copper layer. The chosen discretization is sufficient to ensure a good frequency response of the measured temperature due to surface heat flux fluctuations up to the highest frequencies of about 7.5 kHz we would like to resolve. This choice of the upper limit of the frequency is discussed in more detail below. The order of the model is $n_N = 2206$.

2.2. Parameterization of unknown heat fluxes

The unknown surface heat flux is an infinite dimensional function $\hat{q}(\mathbf{x}, t)$ of the surface coordinates $\mathbf{x}$ and time t. Only

a limited number of n_M local temperature measurements concatenated in the vector $\mathbf{T}_M(t)$ (or $\mathbf{T}_M(s)$ in the frequency domain representation) is available. The unknown heat flux on the boiling surface is therefore spatially parameterized. For this purpose, we introduce

$$\hat{q}(\mathbf{x},t) = \sum_{k=19}^{19+n_Q} \hat{q}_k(t)\Phi_k(\mathbf{x}) \tag{3}$$

for the row with microthermocouples 19–24 [7]. Linear basis functions $\Phi_k(\mathbf{x})$ approximate the unknown heat fluxes as shown in Fig. 4. n_Q denotes the number of heat flux coefficients $\hat{q}_k(t)$ which have to be estimated. In the frequency domain representation (e.g. in Eq. (2)), these fluxes are concatenated in $\mathbf{Q}(s)$. In our case $n_Q = n_M = 6$ which satisfies the necessary condition $n_M \geqslant n_Q$ for the solvability of the IHCP. This parameterization is chosen to ensure optimal input observability of the unknown heat flux coefficients $\hat{q}_k(t)$ for the given fixed microthermocouple locations. This can be achieved with Hankel singular value maximization [14].

2.3. Model reduction

Heat conduction models generally have fast decaying Hankel singular values. Exact inversion is therefore only possible for models of order less than 50–60. Hence, model reduction has to be employed prior to inversion. A non-iterative method of the SLICOT numerical library is used here [18]. A reduced order model with 36 states is obtained which approximates the frequency response of the original model of order $n_N = 2206$ very well up to the highest frequency of 7.5 kHz we would like to resolve.

Non-iterative model reduction methods typically scale with n_N^3 in computational complexity. The order of the full two-dimensional FE-model is already $n_N = 2206$ due to the large number of elements that must be used to resolve the thin gold and copper layer, since the length scales involved in the problem range between 1.0 mm and 1.0 μm. Whereas for simulation purposes such a model order is relatively low, for non-iterative model reduction it is close to the computational limit. Reduction of models of orders above $n_N = 3000$–4000 becomes quickly computationally intractable even if high-performance computing is employed.

We have therefore limited the computational domain to two dimensions, but we resolve the thin gold and copper layer. This is preferable to employing a three-dimensional FE-model of the microthermocouple array which neglects the thin gold and copper layer because it would not yield the desired accuracy at high frequencies. Furthermore, a three-dimensional model involving the thin gold and copper layer would result in a model on the order of $n_N = 50000$–100000 which is beyond our computational capabilities regarding model reduction.

2.4. Solution of the IHCP

For the solution of the IHCP, the reduced heater model must be inverted. An exact inverse is calculated using an algorithm proposed by Silverman [19]. For regularization of the IHCP, a lowpass filter of order 3 with a cut-off frequency of 7.5 kHz has been chosen. The choice of the order and the cut-off frequency is motivated by the temperature measurements, which are filtered with the same cut-off frequency during data acquisition in the experiment. Therefore, no useful frequency component above the cut-off frequency can be expected to be contained in the measurements anyway. By choosing the same cut-off frequency in the IHCP we can assure to resolve the highest frequency component contained in the measured temperature signals. However, there will be errors in the estimates which are due to our modeling approach. In particular, the dimensional reduction of the heat transfer problem from three to two spatial dimensions will limit the accuracy of the estimates in the lower frequency range in a way which is difficult to quantify. The high frequency resolution is a definite advantage compared to our previous works. These issues are discussed in more detail below. A solution of a 3D-IHCP has already been presented before [20] to interpret temperature fluctuations in boiling. However, the frequency resolution was limited by the relatively coarse grids of the discretization which had to be employed in order to render the problem computable. Here, our goal is to achieve a much higher frequency resolution and a good compromise between all factors which have an influence on the quality of the estimate, i.e. the spatial and temporal discretizations, the order of the reduced model, the parameterization of the boundary heat fluxes with respect to the sensor positions as well as the choice of the filter parameters. Details on this matter are thoroughly discussed in [14].

2.5. Estimated local surface heat flux and temperature fluctuations

The temporal and spatial evolution of the estimated surface heat flux and temperature distribution across the boiling surface differs significantly among the boiling regimes.

In low heat flux nucleate boiling, the temporal and spatial heat flux and surface temperature fluctuations are relatively moderate in boiling of isopropanol. The surface temperature exhibits fluctuations between 0.1–0.3 K. At higher heat fluxes in nucleate boiling, both the number of fluctuations per unit time as well as their amplitude increase. Towards critical heat flux, periods of monotonically increasing temperature with excursions up to 1.0–3.5 K can be observed to emerge in an irregular pattern. The temperature excursions mostly extend locally only over one or a few microthermocouples. They are accompanied by relatively steep temperature drops with gradients up to 5000–10000 $\mathrm{K}\cdot\mathrm{s}^{-1}$ during which the temperature drops below the spatial average temperature at the respective operating point.

The number density of temperature excursions and the following temperature drops increases dramatically towards CHF. The number density exhibits its maximum around CHF. The spatial extension of phases with high temperature continues to grow from high heat flux nucleate to transition boiling. Since time and space scales are coupled by the velocity of the wetting and rewetting process, this behaviour implies that the number

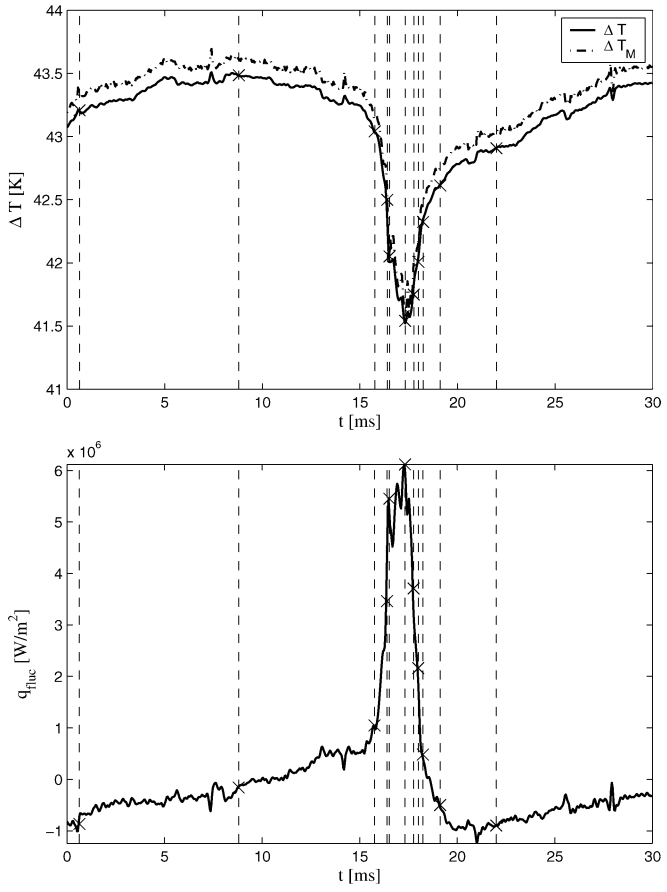

Fig. 5. Estimated surface temperature superheat ΔT and measured temperature superheat ΔT_M during rewetting of the boiling surface in transition boiling (top) and complying estimated peak boiling heat flux fluctuation q_{fluc} (bottom).

density of the occurrence of temperature excursions decreases when observing the fluctuations locally over time. The maximum amplitude of the temperature excursions is reached in the high heat flux transition boiling region and at CHF.

A typical measured temperature excursion with a sudden temperature drop is shown in Fig. 5 together with the estimated surface temperature for an operating point in transition boiling at a superheat of 42.5 K. The complying heat flux estimate is shown below.

The same single fluctuation as in Fig. 5 is shown in the $q_{fluc}/\Delta T$ phase plot in Fig. 6. A strong correlation of the localized heat flux with local superheat inherent in the dynamics of the boiling process is found. The symbols $\times$ denote time instances that correspond with those in Fig. 5. The $q_{fluc}/\Delta T$ cycle starts with a superheat of about 42.5 K at $t = 0.64$ ms. During approx. 8 ms the superheat rises about 0.9 K to reach its maximum in the cycle of about 43.5 K. In the next 7 ms the superheat decreases slightly due to some heat which is withdrawn from the boiling surface. Then, within the very short time period of about 1.5 ms the surface temperature drops sharply. A peak heat flux of 6.0 MW·m^{-2} is identified at the time of the occurrence of the superheat minimum of about 41.5 K. Within the next 2 ms the superheat again rises to about the average superheat of about 42.5 K. It may then take 10–200 ms until the next cycle can be observed.

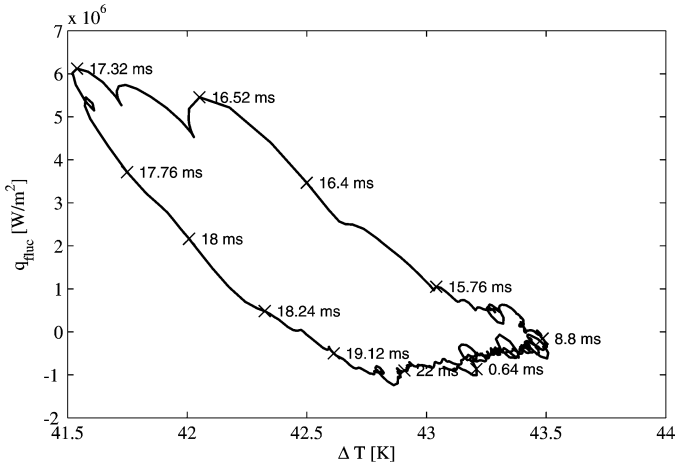

Fig. 6. Phase plot of estimated surface temperature difference and heat flux fluctuation in transition boiling during possible rewetting of the boiling surface.

Very similar patterns like the single fluctuation shown can be repeatedly identified from the measurements. Typical amplitudes of the estimated heat flux fluctuations q_{fluc} in these patterns range between 5–8 MW·m^{-2} at CHF and in transition boiling. In high heat flux nucleate boiling, these amplitudes are typically 3–5 MW·m^{-2} which is about half of those observed in transition boiling. The magnitude of these fluctuations is therefore a feature of a particular boiling regime. In nucleate boiling the temperature drops and the associated high heat fluxes are presumably caused by rapid local evaporation and microconvection of superheated liquid at the boiling surface probably due to similar mechanisms proposed in the microlayer theory. In transition boiling, they are most likely caused by liquid contacts rewetting highly superheated and vapor-covered surface spots at the surface. This generates ideal heat transfer conditions for intense evaporation. As already pointed out, the fluctuations in nucleate boiling are usually observed only for a few microthermocouples. Hence, they extend only over an area which is smaller than the whole microthermocouple array whereas in transition boiling the fluctuations mostly extend over an area which is larger than the 1×1 mm^2 microthermocouple array. Therefore, the characteristic sizes of the liquid-vapor structures in the two-phase at the surface are found to increase with increasing superheat. This is discussed in more detail in Chapter 3.5 where the interfacial vapor–liquid geometry is identified from two-phase flow experiments. It is interesting that the q_{fluc} and ΔT oscillations are correlated in a cyclic manner. As shown in [21], local dry spots might trigger a temperature wave propagation across the heaters and ultimately cause the transition from nucleate to film boiling if no control system as in the present experiments is applied. Therefore the temperature excursions and drops must be subject to further investigations together with the two-phase flow phenomena.

As can be seen from the temperature and heat flux estimates, the high-frequency characteristics of the signals are well preserved. The measured and estimated surface temperature exhibit nearly the same dynamics. This shows that the damping due the sputtered gold and copper layer is very small, else we would observe a significant time delay between the measured

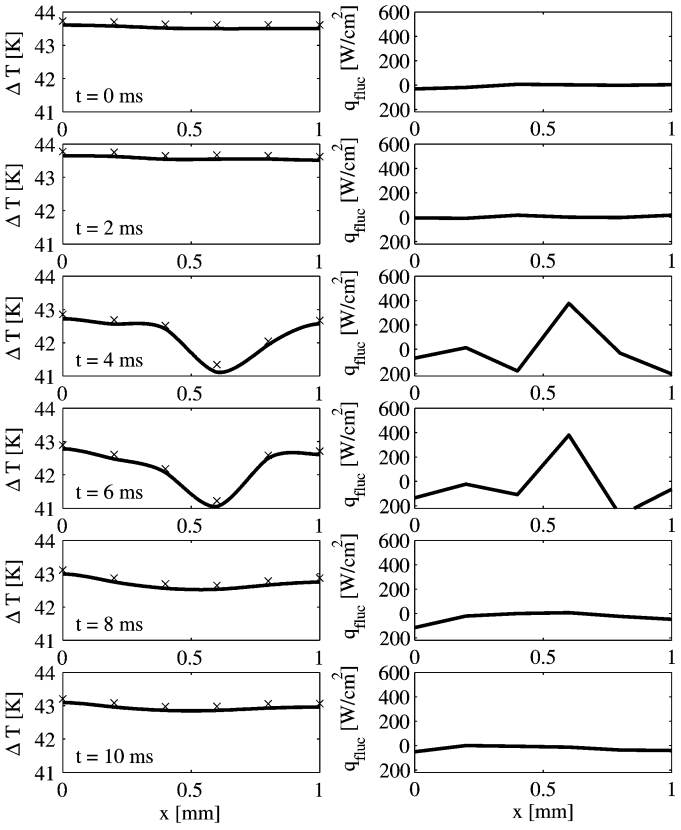

Fig. 7. Time series of estimated surface temperature and heat flux distributions (solid lines) across the computational domain. The measured temperature superheat ΔT_M at the respective measurement positions is denoted by symbols (×).

wall and estimated surface temperature. It can also be concluded that the solution of IHCP is capable of following the fast dynamics of the measured signals. We have also assured this property by testing our algorithm with artificially generated test signals. The surface temperature is estimated to be approximately 0.1 K below the measured wall temperature. Since this difference is on the order of the absolute measurement error of the microthermocouples, it can be concluded that microthermocouple setup is capable of almost measuring the real surface temperatures within these errors and if no higher frequencies components than 7.5 kHz prevail in the boiling process dynamics which the measurement setup cannot resolve. The solution of the IHCP does therefore not add any value to the measured temperature, except that it proves that there is no significant difference in the dynamics and absolute values between the estimated surface and measured wall temperature. Anyway, the solution of the IHCP is needed to estimate the surface heat flux distribution.

A short sequence of estimated heat flux and temperature profiles along the surface boundary computed from the IHCP together with the measured wall temperature is exemplarily shown in Fig. 7. This sequence gives an impression on the fluctuations across the line of the microthermocouple array. It is taken at the same operating point in transition boiling at a superheat of 42.5 K as the fluctuation discussed above. However, we have chosen a sequence here, where the rewetting process occurs very localized at around $x = 0.6$ mm. As can be seen, the surface superheat is almost constant along the heater surface at a level of 44 K during the first 2 ms of the sequence. The negligible spatial variation indicates a two-phase flow structure (probably vapor) larger than the extension of the microthermocouple array. At around 3 ms, the temperature begins to drop along the computed surface boundary with a distinct minimum of about 41.0 K at approximately $x = 0.6$ mm. This local minimum is most probable due a small liquid drop rewetting the surface. As can be seen from the estimated heat fluxes, they correspond exactly to the shown surface temperature profiles. The rewetting process causes a heat flux of 400 $\mathrm{W{\cdot}cm^{-2}}$ which is withdrawn from the surface in the particular rewetted region at $x = 0.6$ mm. Typically, the heat flux fluctuations on the line which are estimated due to background fluctuations without distinct temperature drops or due to slow temperature excursions are in the range of about ± 50 $\mathrm{W{\cdot}cm^{-2}}$ for comparison. The peak heat fluxes identified are hence about a factor 5–10 higher than the background fluctuations.

Before and after the excursion, the heat flux is close to zero or even slightly negative indicating heat transfer from the fluid to the wall at a very low heat transfer coefficient. Negative heat fluxes are probably an artefact of the estimation. These are estimated because of the finite spatial domain which is employed in the solution of the IHCP. In the formulation of the IHCP, heat is only allowed to be exchanged at the boiling surface. Across all other boundaries a zero heat flux boundary condition has been described (cf. Fig. 4). If a strong heat flux occurs locally at the boiling surface boundary, an opposite heat flux has to occur somewhere else at the boundary in order to compensate the imbalance of energy. This effect is more pronounced at the left and right edges of our computational domain where we lack better information on the real lateral boundary heat fluxes and where we do not have measurements to deduce the lateral fluxes from. However, this influence is compensated and damped towards the middle of the computational domain where the thermal energy stored in the heater is only influenced by better estimates of the overall temperature and boundary heat flux distribution. Therefore, the estimation quality increases going farther away from the boundary edges where no validated information is available. A similar effect as the "edge effect" is expected from the dimensional reduction from three to two spatial dimensions of the computational domain of the heat transfer problem. Actually, we would have enough measurement information to avoid this dimensional reduction. However, as already stated, we cannot employ this information currently as we have to limit the dimensional complexity because of the computational limit we are facing with the model reduction routines. Therefore, the estimated peak heat fluxes mentioned should not be considered as absolute values. Rather they must be interpreted as heat flux fluctuations around a mean zero heat flux level during a phase when no temperature fluctuation occurs. Indeed, during these phases the estimated heat flux is close to zero. Any higher negative heat flux is probably not due to physical phenomena, but an error due to the finite domain employed as a model for the IHCP. What is required in the future is the formulation and solution of a IHCP, possibly three-dimensional, by either em-

ploying measurements which are arranged in such a manner that all unknown boundary heat fluxes can be well grasped or by extending the computational domain up to those boundaries where the heat flux distribution is well known.

Despite these limitations, the results clearly suggest that highly localized superheat and heat flux fluctuations at the boiling surface play an important role in the overall boiling mechanism. Although it seems rather likely from these results that local evaporation is the cause for the observed fluctuations, only corresponding optical probe measurements in the two-phase, on the detail of individual and corresponding events, can give more insight to substantiate this conjecture, e.g. if the observed peak heat fluxes which are identified correlate with vapor, liquid or the presence of an interface. Unfortunately, corresponding measurements in both the heated wall and the two-phase flow which allow to correlate the patterns observed in the heater and fluid phase measurements are not available yet as the optical probe cannot be positioned with sufficient precision with respect to the microthermocouple array. However, optical probe measurements can be carried out along with microthermocouple measurements at corresponding operating points along the entire boiling curve [7]. Therefore, the optical probe measurements can be related to the microthermocouple measurements in an averaged sense. These optical probe measurements are used in the following chapter to identify the interfacial geometry of the two-phase flow and to correlate the geometry of the interface with the boiling heat flux. By this approach, we want to clarify if evaporation and microconvection at a vapor–liquid front, namely at the interface, close to the boiling surface is an important mechanism not only for nucleate boiling but for the entire boiling curve.

3. Identification of geometric statistics of two-phase flow

As pointed out before, the presence of a liquid–vapor interface close to the boiling surface is suspected to provide the key mechanism for heat removal in the boiling process. The wetting structure itself as well as their typical dimensions close to the boiling surface are still subject to debate. For a better mechanistic understanding and verification of heat transfer models, an important goal is to identify this information from experimental data of an optical probe together with a mathematical model for the interfacial geometry. A methodology for the identification has already been presented in [8] along with a simple geometry model capturing candidate geometries in a unifying manner. Since the unknown parameters quantifying the wetting structure must be inferred from measured quantities like the vapor fraction and contact frequency, the identification of the interfacial geometry can be formulated as the constrained nonlinear regression problem

$$\min_{\Theta} \sum_{k} \left(\mathbf{y}(\Theta, \Delta T_k) - \mathbf{y}_M(\Delta T_k)\right)^2 \tag{4}$$

$$\text{s.t. Eqs. (6)–(8), (22)–(25)} \tag{5}$$

whose optimal solution minimizes the sum of quadratic differences between the values $\mathbf{y}$ predicted by the model (given below in Eqs. (6)–(8), (22)–(25)) and the real measured values $\mathbf{y}_M$ at $k = 1, 2, \ldots$ different superheats ΔT_k. The measurements considered are the time-averaged vapor fraction and contact frequency above the heater.

In [8], it has been shown in detail how experimental optical probe data must be interpreted in terms of two-phase flow averaging theory. In addition, a model for the identification of the wetting structure has been presented. We will summarize these results here and focus on the new aspects of the identification method. These are concerned with a refined parameterization to describe the dependency of the unknown geometrical dimensions of the wetting structure on the superheat and the possibility to measure the contact angle in-situ if a suitable four-sensor probe was available.

3.1. Geometry model

Consider the specific geometry shown in Fig. 8, which shows a "vapor chunk" with a strongly simplified and idealized interfacial geometry at the boiling surface. This interfacial geometry neglects curvature along the z-direction, but considers the contact angle ϕ of the wetting liquid. If a cutting plane at a position Δz parallel to the boiling surface is introduced, the geometry shown in Fig. 9 results. As discussed in [8], any other geometry, e.g. a bubble, would have yielded the same results for the key averaged geometrical quantities which we are going to employ.

The geometry is parameterized by two characteristic dimensions, the diameter d_S of a vapor chunk and the distance L between vapor chunks, and by the contact angle. We assume N vapor chunks close to a heater surface of area A_H which is

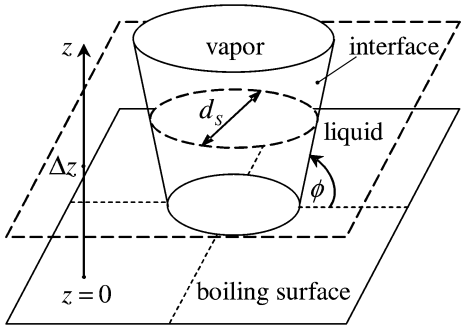

Fig. 8. Three-dimensional interfacial geometry model with a planar interface.

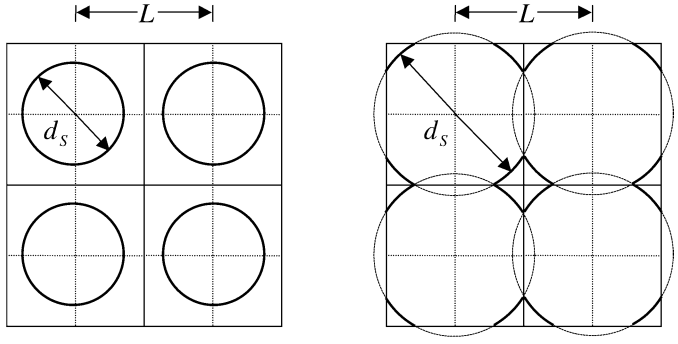

Fig. 9. Interfacial geometry model for the cutting plane at Δz (see Fig. 8): without coalescence (left), with coalescence (right).

assumed to be quadratic. For this specific geometry, volume-averaged quantities, i.e. vapor fraction and interfacial area density, can be computed. These equations apply the general definitions of the averaging theory of multiphase flows originally introduced by Delhaye [11] and others to the geometry in Figs. 8 and 9. We assume that coalescence occurs at $1 < d_S/L \leqslant \sqrt{2}$. No coalescence is assumed to be possible for $0 \leqslant d_S/L \leqslant 1$. The interfacial area density A_i and vapor fraction α_V are given by the model equations

$$A_i = g_1(d_S, L, \phi) \tag{6}$$

$$\alpha_V = g_2(d_S, L) \tag{7}$$

with functions g_1 and g_2 derived in [8]. For the geometry model to be valid, we have to request

$$0 \leqslant d_S/L \leqslant \sqrt{2} \tag{8}$$

because for $d_S/L = 0$ no vapor spots exist and for $d_S/L = \sqrt{2}$ the vapor spots are fully coalesced. The number of nucleation sites N may also be expressed as $N/A_H = L^{-2}$ in this model. A nucleation site is understood as the center of the circular vapor chunk.

The model assumes a particular geometry with particles of equal shape and relative position. Three parameters d_S, L and ϕ are required to completely describe the situation. Obviously, the true wetting structure is much more complicated and changes dramatically along the boiling curve. First, the true interface of a single vapor chunk will be much more irregular in the upper nucleate and transition boiling regimes. Second, the structures will not be of a single type with a regular spatial organization. Consequently, these parameters should be understood as *expected values of yet unknown statistical distributions* of at least the parameters d_S, L and ϕ. This model is introduced to idealize and simplify the much more complex actual interfacial structure of the two-phase flow. It can be considered as a minimum parameter model for identifying a boiling process geometry. It must be understood to equivalently represent the much more complicated wetting behaviour in an averaged sense. As a consequence *the identified parameters d_S and L may not be interpreted to describe a single event of the process since the spatial scales of a single event may vary by orders in magnitude over time and may show a much more complicated geometrical shape*. If the geometry model is applied along the boiling curve, the parameters become functions of superheat.

It has been shown in [8] that the interfacial area density depends on the contact angle of the wetting fluid. In contrast, line density does not. Interfacial area density A_i and line density L_i are related by the contact angle ϕ according to

$$\frac{L_i}{A_i} = \sin\phi \tag{9}$$

at any position z of the cutting plane. At the boiling surface, i.e. at $z = 0$, the same result as in Eq. (9) would have been obtained for geometries with an *arbitrary curvature*, e.g. if we had assumed a bubble geometry.

3.2. Interpretation of multi-sensor probe measurements

Sensor probes ideally measure the phase indicator function $X(\mathbf{x}, t)$ which signals the presence of the vapor (V) or liquid (L) phase at the sensor tip location $\mathbf{x}$ at time instance t. Mathematically, this can be expressed as

$$X(\mathbf{x}, t) = \begin{cases} 0 & (\mathbf{x}, t) \in L \\ 1 & (\mathbf{x}, t) \in V \end{cases} \tag{10}$$

The phase indicator function carries *two independent* pieces of information over time: the time instance of a change of phase and the time duration of the presence of a particular phase.

The vapor fraction α_V is determined in terms of time averaging as

$$\alpha_V = \frac{1}{\Delta\tau} \int_t^{t+\Delta\tau} X \,\mathrm{d}t \tag{11}$$

Ishii [9] suggests to determine the interfacial area density A_i from

$$A_i = \frac{1}{\Delta\tau} \sum_j \left(\frac{1}{|\mathbf{v}_i \cdot \mathbf{n}_i|} \right)_j \tag{12}$$

where the summation is taken over all j instances of interfacial contacts at location $\mathbf{x}$ during the time interval $\Delta\tau$. $\mathbf{v}_i \cdot \mathbf{n}_i$ is the scalar product of interfacial velocity $\mathbf{v}_i$ and the normal vector $\mathbf{n}_i$ of the interface at location $\mathbf{x}$. This product will also be denoted by $v(\mathbf{x}, t)$, the normal interfacial velocity. This equation is based on the theory of two-phase flow where the interface is assumed to have negligible thickness. The interfacial area density A_i can be inferred from four-sensor probe measurements [22]. However, the capabilities of a four-sensor probe extend beyond the measurement of the interfacial area density which is related to the normal interfacial velocity $v = \mathbf{v}_i \cdot \mathbf{n}_i$. We will show subsequently that not only the scalar product $\mathbf{v}_i \cdot \mathbf{n}_i$ can be measured, but also the normal vector $\mathbf{n}_i$ itself. Furthermore, since the normal vector is closely related to the contact angle of the wetting fluid, the contact angle can be measured using a four-sensor probe.

For this purpose, we assume that the interface is large compared to the size of the probe array and does not deform during sensor contact. The first assumption also implies that the interface curvature is small compared to the size of the probe array. Fig. 10 shows an example of such a probe. Further, we assume that each individual interface j passes all four sensor tips. Hence, four time instances τ_l, $l = 1, \ldots, 4$, at which the interface passes each sensor can be detected.

A four-sensor probe represents a system with a minimal number of sensors that spans a local reference coordinate system for the interfacial movement in three-dimensional space. It can also be viewed as a system of six double-sensor probes when combinations of two of the four sensors are considered at a time. For each double-sensor probe $k = 1, \ldots, 6$ we can write

$$v\Delta\tau_k = \Delta s_k \mathbf{n}_i \cdot \mathbf{n}_{s,k} \tag{13}$$

where

$$\Delta\tau_k = \tau_l - \tau_m, \quad l = 1, \ldots, 3, \; m = l + 1, \ldots, 4 \tag{14}$$

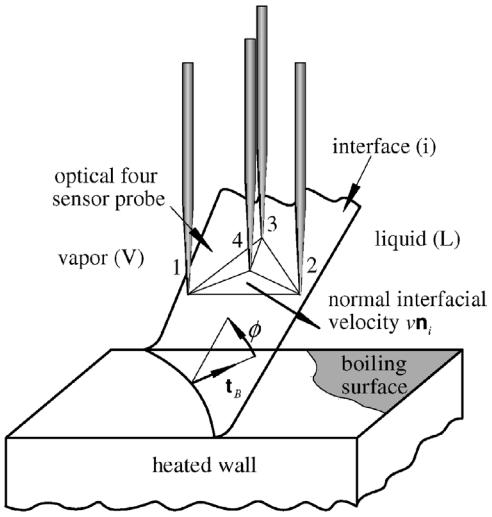

Fig. 10. Example a four-sensor probe for measuring $\mathbf{n}_i$ and v.

is the time difference for the interface to travel from sensor l to sensor m and

$$\Delta s_k = \mathbf{s}_k \cdot \mathbf{n}_{s,k} = |\mathbf{s}_k| = |\mathbf{s}_l - \mathbf{s}_m| \quad l = 1,\ldots,3,\ m = l+1,\ldots,4 \tag{15}$$

is the known distance between sensor l and sensor m. $\mathbf{n}_{s,k}$ is the unit vector pointing in the measurement direction of each double sensor. To obtain a solution for v and $\mathbf{n}_i$ at least three of the six distances $\Delta\mathbf{s}_k$ must be known. In order to minimize unavoidable measurement errors in the solution, it is advantageous to measure all six distances and to solve an overdetermined set of equations in a least-squares sense. The problem can be cast into

$$\frac{1}{v}(\mathbf{N}_s\mathbf{n}_i)^{\mathrm{T}}\mathbf{v}_s = 1 \tag{16}$$

with

$$\mathrm{N}_s = \begin{bmatrix} \mathbf{n}_{s,1}^{\mathrm{T}} \\ \mathbf{n}_{s,2}^{\mathrm{T}} \\ \vdots \\ \mathbf{n}_{s,6}^{\mathrm{T}} \end{bmatrix}, \qquad \mathbf{n}_i = (n_{ix}, n_{iz}, n_{iz})^{\mathrm{T}}$$

$$\mathbf{v}_s = \left(\frac{\Delta s_1}{\Delta\tau_1}, \frac{\Delta s_2}{\Delta\tau_2}, \ldots, \frac{\Delta s_6}{\Delta\tau_6}\right)^{\mathrm{T}} \tag{17}$$

by assembling Eq. (13) for each double-sensor probe k. $\mathbf{N}_s$ is the matrix of unit vectors of the measuring direction of the double-sensors and $\mathbf{v}_s$ is the vector containing the sensed velocity of each double sensor. These quantities are known or measured. $\mathbf{n}_i$ is the normal vector and is unknown. Since the normal vector has unit length, Eq. (16) can be solved as the minimization problem

$$\min_{\mathbf{n}_i, v}\left|\frac{1}{v}(\mathrm{N}_s\mathbf{n}_i)^{\mathrm{T}}\mathbf{v}_s - 1\right| \tag{18}$$

$$\text{s.t. } |\mathbf{n}_i| = 1 \tag{19}$$

where the unit length of the normal vector is expressed as an equality constraint in the minimization problem. The solution of this minimization problem yields the normal interfacial velocity v whose inverse has been shown to be the interfacial area density [23,24], and the vector $\mathbf{n}_i$ normal to the interface. This way, one is able to identify the local orientation of the interface in three-dimensional space together with its normal velocity from four-sensor probe data.

The "local contact angle" ϕ at the probe tip at position z above the surface equals the apparent contact angle at the boiling surface $z = 0$ if the interfacial geometry does not change curvature along z. Under this assumption, ϕ can easily be obtained from the projection of $\mathbf{n}_i$ onto the unit vector $\mathbf{t}_B$ parallel to the boiling surface according to

$$\phi = \arcsin(\mathbf{n}_i \cdot \mathbf{t}_B) \tag{20}$$

with $\mathbf{t}_B$ normal to the cutting line which is defined by vapor–liquid the interface and the boiling surface. Hence, for a fixed interfacial velocity $\mathbf{v}_i$ of a material point on the interface, the normal interfacial velocity v and the interfacial area density depend on the contact angle according to

$$v \propto \sin\phi, \qquad A_i \propto \sin^{-1}\phi \tag{21}$$

3.3. Interpretation of single sensor probe experiments

Buchholz et al. [25] have employed a four-sensor optical probe where the axial distance between the two lowest sensor tips is 160 μm. Since in his studies it is not the goal to measure the interfacial area density or the velocity locally as outlined above, the axial distance of the two sensor tips is large compared to the smallest distance between the lowest sensor tip of the probe and the boiling surface which in his experiments has been 8 μm. Therefore, data from the lowest sensor tip is employed here and an approximation for the interfacial area density according to Eq. (12)

$$A_i = \frac{f}{v_C} = \frac{N_p}{v_C\Delta\tau} \tag{22}$$

is introduced [8]. The contact frequency f replaces the summation over all instances j in Eq. (12) under the assumption that the normal interfacial velocity v_j is the same for all j instances and that it equals a normal characteristic interfacial velocity v_C which is unknown. The contact frequency is the ratio of the number of phase changes N_p and during the measurement interval $\Delta\tau$. As discussed already in [8] the contact frequency may also be interpreted as the interfacial area density flux which equals the time rate of change of the vapor fraction. Hence, the contact frequency may also be considered as a rate of evaporation.

Recent experimental results by Buchholz et al. [7] indicate typical characteristic velocity of the two-phase flow between 400 mm·s^{-1} and 1000 mm·s^{-1} at a distance between 4.5 mm and 20 mm to the boiling surface obtained by cross-correlating the characteristic functions. If this data is extrapolated linearly to the boiling surface, a characteristic velocity of approx. 200 mm·s^{-1} is obtained. It might serve as a first clue on the magnitude of the interfacial velocity. Further verification can only be achieved by employing appropriately designed multi-sensor probes for measuring local interfacial velocities as out-

lined in Section 3.2. Both measured contact frequency f_M and vapor fraction $\alpha_{V,M}$ are included in the measurement vector

$$\mathbf{y}_M(\Delta T_k) = \begin{pmatrix} A_{i,M}(\Delta T_k) \\ \alpha_{V,M}(\Delta T_k) \end{pmatrix} = \begin{pmatrix} f_M(\Delta T_k)/v_C \\ \alpha_{V,M}(\Delta T_k) \end{pmatrix} \tag{23}$$

The index k denotes the measurement samples at different operating points along the boiling curve.

3.4. Parameterization of interfacial geometry as a function of superheat

The geometrical model (6)–(8) predicts the area densities A_i and vapor fraction α_V and is written as

$$\mathbf{y} = \begin{pmatrix} A_i(\mathbf{p}) \\ \alpha_V(\mathbf{p}) \end{pmatrix} = \begin{pmatrix} g_1(\mathbf{p}) \\ g_2(\mathbf{p}) \end{pmatrix} \tag{24}$$

It depends on the diameter d_S and the distance L which are combined in the geometrical parameter vector $\mathbf{p} = (d_S, L)^{\mathrm{T}}$. Note, that we have not included the contact angle ϕ in the parameter vector $\mathbf{p}$ since ϕ is not identifiable from single sensor probe data which we are going to employ. Instead, the contact angle ϕ is lumped into the unknown characteristic velocity v_C.

If the model (6)–(8) is applied along the entire boiling curve, the geometrical quantities contained in the parameter vector $\mathbf{p}$ become functions of superheat ΔT. Within the constraints given by Eq. (8), both d_S and L could in principal behave arbitrarily. In order to identify the unknown dependency of $\mathbf{p}$ with superheat ΔT, a parameterization must be chosen for $d_S(\Delta T)$ and $L(\Delta T)$ that captures the essential behaviour of the physics, but is adapted suitably to the number of experimentally available data points. In contrast to [8], where a linear dependency has been chosen, because the experimental data has not allowed a finer parameterization, we here employ quadratic spline functions [26] which we denote with f_1 and f_2, respectively, to correlate d_S and L with the superheat ΔT. The parameter vector Θ concatenates the parameters of the spline function. This finally leads us to

$$\mathbf{p}(\Delta T) = \begin{pmatrix} d_S(\Delta T) \\ L(\Delta T) \end{pmatrix} = \begin{pmatrix} f_1(\Theta, \Delta T) \\ f_2(\Theta, \Delta T) \end{pmatrix} \tag{25}$$

3.5. Identification of the interfacial geometry

The parameter estimation problem (4)–(5) is solved using a sequential quadratic programming method [27].

Comparison between experimental data and the model regression is shown in Fig. 11 and 12 for an assumed characteristic velocity $v_C = 200$ mm·s^{-1}. Although, the interfacial area density depends on the chosen characteristic interfacial velocity, the goodness of regression is not changed when other characteristic interfacial velocities are chosen. As can be expected and discussed in more detail below, the average size of vapor chunks and their distance to each other depend on the characteristic velocity chosen. The contact frequency is obtained from the raw probe data based on an extended two-level threshold method [7]. As can be seen from the measurements points shown in the figures, the scatter in the averaged data is not significant when averaging the probe data at each operating point over five subsequent time intervals of 5 s each.

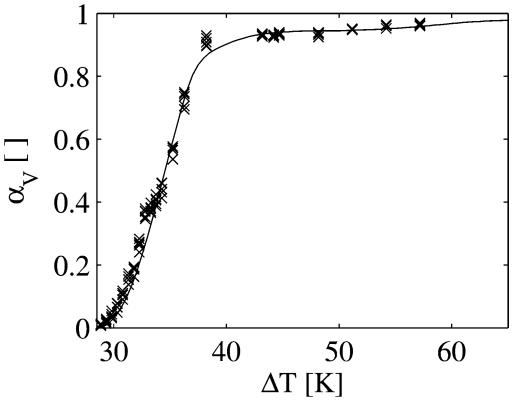

Fig. 11. Comparison between measured (× symbols) and predicted (solid line) vapor fractions for $v_C = 200$ mm·s^{-1} for boiling of isopropanol at 8 μm.

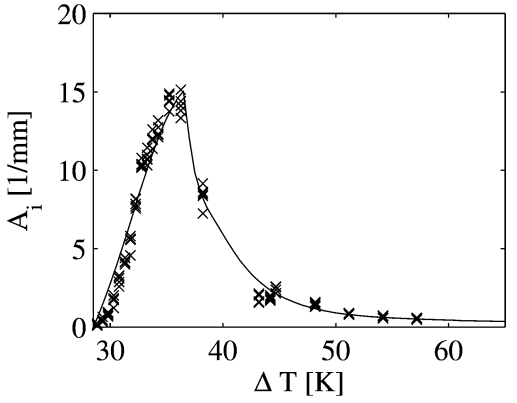

Fig. 12. Comparison between measured (× symbols) and predicted (solid line) interfacial area densities for $v_C = 200$ mm·s^{-1} for boiling of isopropanol at 8 μm.

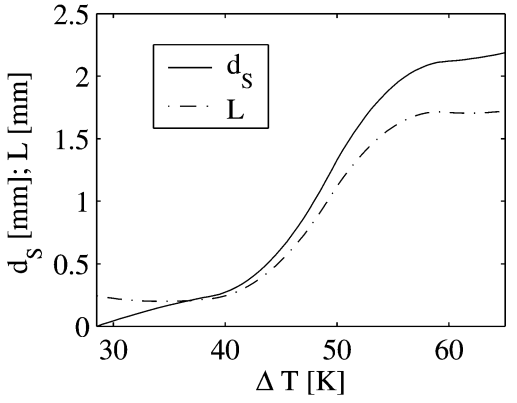

Fig. 13. Estimated vapor chunk size and spacing during boiling of isopropanol for $v_C = 200$ mm·s^{-1}.

Fig. 13 shows the identified geometric parameters d_S and L as a function of the superheat ΔT. Close to the onset of boiling, the estimated average vapor chunk diameter d_S is close to zero, it grows toward higher superheats and saturates in the film boiling region. At CHF at about $\Delta T = 35$ K, the average spacing L and the diameter d_S are equal and in an averaged sense, the interfaces begin to coalesce. In the high heat flux transition boil-

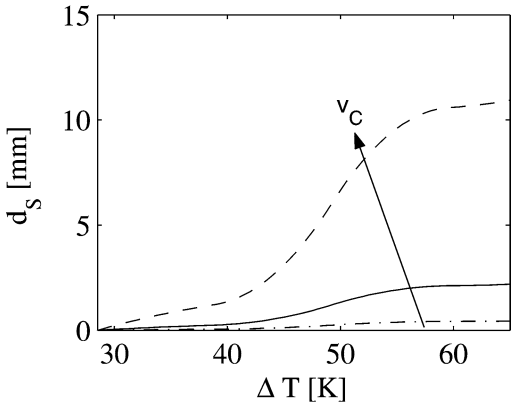

Fig. 14. Estimated vapor chunk size during boiling of isopropanol for $v_C = \{40, 200, 1000\}$ mm·s^{-1}.

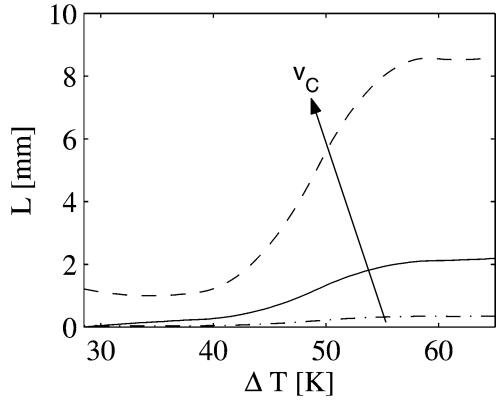

Fig. 15. Estimated vapor chunk spacing during boiling of isopropanol for $v_C = \{40, 200, 1000\}$ mm·s^{-1}.

ing region the average diameter of a vapor chunk d_S increases as well as the chunk spacing L with increasing superheat ΔT until they level off in film boiling. The results clearly show that the boiling surface accretes with increasing superheat. The vapor chunk diameter d_S and spacing L depend on the chosen characteristic velocity v_C as already pointed out. As shown in [8] and demonstrated in Figs. 14 and 15, the estimates of d_S and L increase proportionally with increasing characteristic velocity v_C. Remember, the identified parameters d_S and L must interpreted in an average sense and not as single event of the process.

Nonetheless, the size of vapor chunks identified from sensor probe data can be confirmed quantitatively by looking closely at periods of high temperatures measured by the microthermocouple array as such periods are probably associated with local dry-out of the surface. In the transition boiling regime we can indeed find periods of high temperature and sudden temperature drops repeatedly which extend simultaneously over the entire microthermocouple array of 1×1 mm^2. Using principal component analysis [28], we find that, in transition boiling, the first principal component can describe almost up to 95% of the measured temperature fluctuations of all microthermocouples of the array. This is another clear indication confirming the results of Fig. 7 that dry-out and rewetting can occur over an area of at least 1×1 mm^2 at the surface and that it is a highly self-similar process. We observe that rewetting occurs in a very short period of time until the wetted surface undergoes dry-out due to evaporation again. As already pointed out this is an intermittent, repeating process.

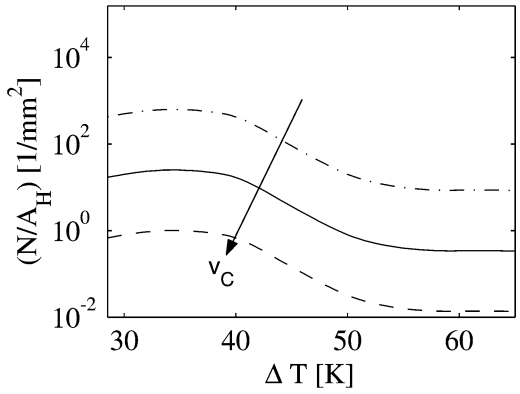

Fig. 16. Estimated nucleation site density during boiling of isopropanol for $v_C = \{40, 200, 1000\}$ mm·s^{-1}.

An estimate of the nucleation site density can be obtained even in boiling regimes where their determination by visual observation is impossible. The concept of nucleation site density is carried over into the transition and film boiling regions by defining it as the center of any vapor chunk along the entire boiling curve. The estimates are shown in Fig. 16 for different values of v_C. First, a slight increase in nucleate site density beginning at the onset of nucleate boiling up to CHF is found. The estimate reveals that the nucleation site density decreases with increasing superheat in transition boiling until it levels off in film boiling. A large characteristic interfacial velocity decrease the nucleation site density.

The results on the identified interfacial geometry of boiling isopropanol are in good agreement with our results for FC-72 [8]. For both fluids, the interfacial geometry model quantitatively predicts the measured probe data very close to the surface well. Even the interrelation as observed experimentally between vapor fraction and interfacial area density is reasonably accounted for by the model despite the unknown interfacial velocity. This interrelation seems to be a distinct feature of the boiling process along the boiling curve. It gives additional confidence in the model and the identified parameters. The estimates for d_S and L in boiling isopropanol are within the same range as those for FC-72. However, the results can only be compared qualitatively, because in this study the dependence of the estimates on the superheat is identified with higher resolution due to the use of spline functions. For both FC-72 and isopropanol, we find that the average size of vapor chunks increases with increasing superheat. The average distance of the vapor structures is found to increase for boiling isopropanol, whereas in our previous study it has been found to decrease with increasing superheat. It remains open if the identified decrease with superheat for boiling FC-72 is due to a physical effect or a consequence of the coarse linear parameterization and the limited experimental data points employed in the previous study.

The estimated equivalent nucleation site densities in boiling isopropanol in the framework of this study range between

1 mm^{-2} and 5×10^2 mm^{-2}. At low heat fluxes they are in reasonable agreement with experimental results of [29,30], although in these investigations propane and R134a have been employed as test fluids. In any case, the results have only been obtained with a characteristic velocity which as been assumed constant, but might change along the boiling curve.

3.6. Correlation of boiling heat flux with interfacial area density

Interfacial area density has been proposed in [8] to be the probably most important factor for a unifying mechanistic model for boiling heat flux in all boiling regimes. Again, we correlate the boiling heat flux with the interfacial area density A_i, or equivalently (cf. Eq. (22)), with the contact frequency f according to

$$q = \overline{C} v_C A_i = C f \tag{26}$$

where C is a constant parameter and includes the unknown characteristic interfacial velocity. Fig. 17 shows the results of the correlation using contact frequency data at a distance of 8 μm above the heater surface. The constant C is found by the solution of a simple regression problem.

Superheat as employed in the correlation for FC-72 [8] is here not required to find a reasonable fit. This difference in the structure of the correlation might be due to the optical probe measurements and the heat flux measurements for FC-72 which have not been carried out simultaneously. As already conjectured in [8], contact frequency can be a self-sufficient measure to correlate boiling heat flux. Obviously, this seems to be true for isopropanol boiling. However, comparing the correlated and the measured heat flux in Fig. 17, we find that large deviations exist. Up to 32 K at low heat fluxes in nucleate boiling and above 50 K in film boiling the correlation underpredicts the measured boiling heat flux by more than 50%. The deviations even increase towards lower superheats in nucleate and towards higher superheats in film boiling. In the region between 32–50 K, which includes the critical point, the deviations are within ±50%. Obviously, the correlation seems to be more suitable in the high heat flux region where most of the heat is transferred

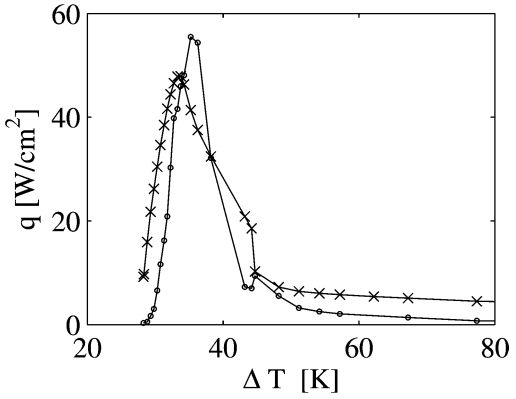

Fig. 17. Correlated isopropanol boiling curve according to Eq. (26) with contact frequency data (∘ symbols) taken at a distance of 8 μm above the heater surface. $C = 0.019$ W·cm^{-2}·s^{-1}. $q/\Delta T$ data denoted by × symbols.

by evaporation at the liquid–vapor interface. On the one hand, the higher deviations of up to 95% in low heat flux nucleate boiling can probably be attributed to convective effects which are due to bubble agitation of superheated liquid and which are not included in the simple correlation proposed. One the hand, the actual interfacial dynamics is much more complex than it could be captured by a simple correlation and by measurements taken only at 8 μm. Although we expect the relevant heat transfer mechanisms, e.g. liquid evaporation, to happen at a distance around a few micrometer above the surface or even closer, there are two important issues to consider. First, at small distances of the probe to the surface, e.g. 8 μm, the probe senses only those phenomena which occur over a very small region at the heater surface due to geometric reasons. These phenomena observed very locally may differ somewhat from the rest of the heater. In addition, the measured boiling curve represents a spatial average of the superheat and boiling heat flux over the entire heater whereas the correlation according to Eq. (26) employs a temporal average of local measurements of the two-phase flow structure. Hence, for optical probe measurements very close to the surface, the assumption of ergodicity may not always be fulfilled completely. This may explain some of the deviations. Second, it remains still open what effect the whole boundary layer of the two-phase flow has on the heat transfer mechanism. We can expect the spatial and temporal scales of the relevant interfacial processes to change along the entire boiling curve. This includes the size of the typical geometric structures above the boiling surface that determine thickness of the boundary layer, for example. Therefore, the relevant mechanisms for heat transfer in the two-phase may not occur at the same distance to the heater for all operating points along the boiling curve, but may depend on the geometric structure. E.g. in film boiling, almost no vapor–liquid fluctuations have been observed at 8 μm whereas at 48 μm distinct, rather regular patterns of liquid–vapor fluctuation of growing and necking bubbles out of the closed vapor film can be found. Here, much of the heat is definitely withdrawn due to the transport of these bubbles. Interestingly, if we take the contact frequency data at 48 μm instead of 8 μm to correlate the boiling curve in film boiling, slightly smaller deviations between the measured boiling curve and correlated boiling curve in film boiling can be found. Although, it can definitely be said that a three-phase contact line does not exist in film boiling, the suspected quantity, interfacial area density, can currently not be determined more precisely, but instead has to be approximated by the contact frequency assuming a constant interfacial velocity along the entire boiling curve. New measurements using multiple sensor probes are required to measure interfacial area densities as a function of ΔT. Such measurements require even more miniaturized probes and elaborate signal processing schemes as pointed out. Considering that the entire boiling curve is correlated with a single parameter, the deviations are acceptable. Even if they are partly very large, the simple correlation seems to capture qualitatively most of heat transfer mechanism along the entire boiling curve quite well. Our results support the hypothesis that the presence and distribution of the liquid–vapor front close to the surface, i.e. the interface, plays a significant role in the overall boiling

heat transfer mechanism. It is obvious from Fig. 11 that the vapor fraction does not correlate with the boiling heat flux at 8 μm. The kink which can be observed in both the measured $q/\Delta T$ and the correlated boiling curve at about 42 K is discussed in [31].

It is interesting to note, that turbulence in single-phase flow can be well correlated using a dimensionless frequency [32], e.g. the Strouhal number. In our context, the contact frequency which is the number of liquid–vapor fluctuation per time, has been interpreted as the area of the liquid–vapor interface per volume using a characteristic velocity. Although the boundary conditions in single-phase turbulent flow and boiling processes are quite different, the interpretation of both the phenomena in the boundary layers simply in terms of time and space scales related by a characteristic velocity is common to both approaches. This property is also closely related to the closure issue for both turbulent flows [32] and multiphase flows [10,33,34]. In the context of multiphase flows and averaging however, the vapor fraction, interfacial area density flux and their evolution have been identified relevant to achieve closure and to restore the lost information due to averaging. Such a closure has basically been achieved here for the boiling process by correlating the interfacial area density in terms of contact frequency with the vapor fraction using a geometric model as well as with the boiling heat flux. Unless a deeper understanding on the relevant phenomena is achieved, the introduction of turbulent effects into the discussion in boiling processes is not yet advisable, but the interrelation between the disciplines and the quite similar problems with closure in both approaches should not be overseen in future investigations.

4. Discussion and summary

This study reveals that unmeasurable quantities, namely the surface heat flux and temperature as well as the interfacial geometry of the wetting structure, needed for a better mechanistic understanding of a boiling processes can be identified successfully from temperature and optical probe measurements. Surface temperature and heat fluxes are estimated from temperature data in the heated wall. The wetting structure close to the surface is identified from optical probe data as a function of the superheat using a simple geometrical model which captures different modeling approaches in a unifying manner. The results presented here for the boiling of isopropanol are in good accordance with results obtained for FC-72 in our previous study [8]. Thus, both data sets support the conjecture that the interfacial geometry of the wetting structure close to and at the surface is of fundamental importance for the development of a mechanistic model of boiling heat transfer. Our studies underline the conclusions drawn by other authors that the interface itself provides a key mechanism in the boiling process to carry away much of the heat from the surface. One aspect are the peak heat fluxes identified in this study in nucleate and transition boiling which exceed the average boiling heat flux by an order of 10^2. Heat fluxes of such an order of magnitude have also been predicted by the microlayer theory [35] for low heat flux nucleate boiling. Dhir and Liaw's unifying model [3] for nucleate and transition boiling also predicts that the local heat transfer is highest in the wedge close to the three-phase contact line for nucleate and transition boiling. However, a three-phase contact line is not present in film boiling. But still, quite a similar mechanism associated with the interface might dominate the heat transfer, e.g. the presence of interface very close to the boiling surface during the necking of the wavy vapor film interface while forming a bubble. However, the detailed physical mechanisms underlying the candidate models are not fully explored. These include thin film adsorption and contact line movement as well as the relevance of the contact angle and of the interfacial velocity. Therefore, it is necessary to extend our methodology in a next step. As pointed out, four-sensor probes can provide the necessary information regarding the influence of the contact angle and interfacial velocity. Such measurements could prove or disprove the hypothesis that interfacial area density is a key parameter in boiling. At the same time, the geometry model of this work should be extended by an energy balance such as in [2] to hopefully better discriminate between the mechanisms proposed by competing models. Temperature measurements in the two-phase flow and in the heated wall as presented by [25] can provide very valuable additional information for this task and should allow to identify the contribution of the suspected local heat transfer mechanisms to the overall heat transfer process in the future.

References

[1] V.P. Carey, Liquid–Vapor Phase-Change Phenomena, Series in Chemical and Mechanical Engineering, Hemisphere, Washington, DC, 1992.
[2] P. Stephan, J. Hammer, A new model for nucleate boiling heat transfer, Wärme- und Stoffübertragung 30 (1994) 119–125.
[3] V.K. Dhir, S.P. Liaw, Framework for a unified model for nucleate and transition pool boiling, J. Heat Transfer 111 (1989) 739–746.
[4] P.C. Wayner Jr, Thermal and mechanical effects in the spreading of a liquid film due to a change in the apparent finite contact angle, J. Heat Transfer 116 (1994) 938–945.
[5] R. Hohl, H. Auracher, J. Blum, W. Marquardt, Characteristics of liquid–vapor fluctuations in pool boiling at small distances from the heater, in: Proc. 11th Int. Heat Transfer Conference, vol. 2, Kyongju, Korea, 1998, pp. 383–388.
[6] R. Hohl, Mechanismen des Wärmeübergangs beim stationären und transienten Behältersieden im gesamten Bereich der Siedekennlinie, PhD thesis, Fortschritt-Berichte VDI, Reihe 3, Nr. 597, VDI Verlag, Düsseldorf, 1999, ISBN 3-18-359703-9.
[7] M. Buchholz, H. Auracher, T. Lüttich, W. Marquardt, Experimental investigation of local processes in pool boiling along the entire boiling curve, Int. J. Heat Fluid Flow 25 (2) (2003) 243–261.
[8] T. Lüttich, W. Marquardt, M. Buchholz, H. Auracher, Towards a unifying heat transfer correlation for the entire boiling curve, Int. J. Thermal Sci. 43 (12) (2004) 1125–1139.
[9] M. Ishii, Thermo-fluid Dynamic Theory of Two-phase Flow, Eyrolles, Paris, 1975.
[10] D.A. Drew, S.L. Passman, Theory of Multicomponent Fluids, Springer, Berlin, 1999.
[11] J.M. Delhaye, Basic equations for two-phase flow modeling, in: Two-Phase Flow and Heat Transfer in the Power and Process Industries, 1981, pp. 40–97.
[12] J. Hadamard, Lectures on Cauchy's Problem in Linear Partial Differential Equations, Yale University Press, New Haven, 1923.
[13] H.W. Engl, Regularization methods for the stable solution in inverse problems, Surveys Math. Indust. 3 (1993) 71–143.

[14] T. Lüttich, A. Mhamdi, W. Marquardt, Design, formulation and solution of multi-dimensional inverse heat conduction problems, Numer. Heat Transfer, Part B 47 (2) (2005) 111–133.

[15] A.N. Tikhonov, V.Y. Arsenin, Solutions of Ill-Posed Problems, V.H. Winston and Sons, 1977.

[16] J. Blum, W. Marquardt, Robust and efficient solution of the inverse heat conduction problem using observers, in: J. Henriette, P. Lybaert, M. El Hayeck (Eds.), Advanced Concepts and Techniques in Thermal Modelling. Proc. Eurotherm Seminar 53, October 1997, pp. 175–182.

[17] J. Blum, W. Marquardt, An optimal solution to inverse heat conduction problems based on frequency domain interpretation and observers, Numer. Heat Transfer, Part B: Fund. 32 (1997) 453–478.

[18] A. Varga, Model reduction routines for SLICOT, Technical Report NICONET Report 1999-8, Working Group on Software WGS, ESAT—Katholieke Universiteit Leuven, 1999.

[19] L. Silverman, Inversion of multivariable linear systems, IEEE Trans. Automatic Control AC 14 (3) (1969) 270–276.

[20] M. Buchholz, T. Lüttich, H. Auracher, W. Marquardt, Pool boiling at high heat fluxes (part I): Local temperature & heat flux fluctuations at the heater surface, in: D. Gorenflo, A. Luke (Eds.), Proc. Int. Refrig. Conf. Comm. B1, Paderborn, October 2001, Session B5.8, pp. 420–429.

[21] J. Blum, T. Lüttich, W. Marquardt, Temperature wave propagation as a route from nucleate to film boiling? in: G.P. Celata, P. Di Marco, R.K. Shah (Eds.), Two-Phase Flow Modelling and Experimentation, Pisa, Italy, May 1999, pp. 137–144.

[22] I. Kataoka, A. Serizawa, Interfacial area concentration in bubbly flow, Nuclear Engrg. Design 120 (1990) 163–180.

[23] I. Kataoka, M. Ishii, A. Serizawa, Local formulation and measurements of interfacial area in two-phase flow, Int. J. Multiphase Flow 12 (4) (1986) 505–529.

[24] S.T. Revankar, M. Ishii, Theory and measurement of local interfacial area using a four sensor probe in two-phase flow, Int. J. Heat Mass Transfer 36 (12) (1993) 2997–3007.

[25] M. Buchholz, H. Auracher, T. Lüttich, W. Marquardt, A study of local heat transfer mechanisms along the entire boiling curve by means of microsensors, Internat. J. Thermal Sci. 45 (3) (2006) 269–283 (this issue).

[26] P. Dierchx, Curve and Surface Fitting with Splines, Oxford University Press, Oxford, 1993.

[27] J. Nocedal, S.J. Wright, Numerical Optimization, Springer, Berlin, 1999.

[28] I.T. Jolliffe, Principal Component Analysis, Springer, Berlin, 1996.

[29] A. Luke, E. Danger, D. Gorenflo, Size distribution of active and potential nucleation sites in pool boiling, in: J. Taine (Ed.), Proc. 12th Int. Heat Transfer Conf., Grenoble, France, 2002.

[30] G. Barthau, E. Hahne, Nucleate pool boiling of R134a on a gold-plated copper test tube, in: D. Gorenflo, A. Luke (Eds.), Proc. Int. Refrig. Conf. Comm. B1, Paderborn, October 2001, Session B5.8, pp. 372–379.

[31] H. Auracher, W. Marquardt, Experimental studies of boiling mechanisms in all boiling regimes under steady-state and transient conditions, Int. J. Thermal Sci. (2002) 586–598.

[32] O. Molerus, The relevance of dimensionless frequencies for turbulent flow phenomena observed in chemical engineering practice, Chem. Engrg. Sci. (2002) 933–938.

[33] J.A. Boure, Two-phase flow models: the closure issue, in: G.F. Hewitt, J.M. Delhaye, N. Zuber (Eds.), Multiphase Science and Technology, vol. 3, Hemisphere, Washington, DC, 1987, pp. 3–30.

[34] D.A. Drew, Evolution of geometric statistics, SIAM J. Appl. Math. 50 (3) (1990) 649–666.

[35] P. Stephan, C. Höhmann, J. Kern, Microscale measurement of wall-temperature distribution at a single vapor bubble for evaluation of a nucleate boiling model, in: Space Technology and Applications International Forum—STAIF 2002, 2002.